EAI Endorsed Transactions
on Sustainable Manufacturing and Renewable Energy Research Article EAI.EU

A Bi-Level Optimization Framework for Solar Concentrator Installation and Prism Layout Design Using Genetic Algorithms

Le Duc Dao[1*] and Nguyen Thanh Loi[2]

[1]School of Industrial Management, Ho Chi Minh City University of Technology (HCMUT), 268 Ly Thuong Kiet Street, Dien Hong Ward, Ho Chi Minh City, Vietnam
[2]Vietnam National University, Ho Chi Minh City, Linh Xuan Ward, Ho Chi Minh City, Vietnam

Abstract

As clean energy systems expand, the efficient installation of solar concentrators is increasingly constrained by the interaction between site layout and internal optical design. This study proposes an integrated bi-level optimization model that jointly determines concentrator installation on a floor plan and the internal prism design of each unit. The framework explicitly considers Blocklight obstructions, standardized concentrator types, internal exits, Total Light Efficiency (TLE), and economic profit. The upper level optimizes concentrator selection, placement, and orientation, while the lower level refines internal prism layouts and exit positions. A nested Genetic Algorithm framework is developed to solve the resulting bi-level optimization problem. Experimental results demonstrate that the framework can produce feasible and economically attractive solutions for solar concentrator deployment in constrained installation.

Keywords: Solar concentrator; Genetic Algorithms; bi-level optimization

Received on 12 April 2026, accepted on 22 October 2026, published on 02 November 2026

Copyright © 2026 Le Duc Dao *et al.*, licensed to EAI. This is an open access article distributed under the terms of the CC BY-NC-SA 4.0, which permits copying, redistributing, remixing, transformation, and building upon the material in any medium so long as the original work is properly cited.

doi: 10.4108/eetsmre.12581

*Corresponding author. Email: lddao@hcmut.edu.vn

1. Introduction

Fossil fuels remain the predominant energy source, accounting for over 80% of global energy consumption. They play a fundamental role in sustaining modern society by powering essential daily activities, including electricity generation, transportation systems, and diverse industrial sectors. Beyond their role as a primary energy resource, the fossil fuel industry serves as a major pillar of economic development, creating extensive employment opportunities and driving national growth. This reliance on fossil fuels has been instrumental in enhancing global living standards and prosperity [1]-[3].

However, fossil fuels are simultaneously identified as the primary drivers of the global climate crisis, accounting for nearly 90% of anthropogenic CO_2 emissions. This excessive carbon output accelerates global warming and intensifies the frequency of extreme weather catastrophes. Furthermore, the utilization of these resources causes severe environmental degradation across air, water, and

soil at every stage of their lifecycle. Such widespread pollution inevitably leads to the decline of vital ecosystems and a significant loss of global biodiversity [4], [5].

Renewable energy sources, particularly solar energy, have emerged as definitive energy solutions of the future. These clean energy alternatives play a pivotal role in mitigating CO_2 emissions and reducing air pollution, thereby significantly improving public health outcomes. By offering a sustainable and efficient replacement for fossil fuels, renewable energy is currently undergoing a transformative transition to become the cornerstone of the global energy landscape [6].

Transitioning energy consumption habits and paradigms does not necessitate the immediate and total elimination of fossil fuels. Instead, a progressive reduction is required, wherein fossil fuels continue to serve as a critical "bridge" in the energy transition. Currently, solar energy has garnered significant attention from both governments and enterprises, a trend that has catalyzed substantial investment from corporations into large-scale, profitable projects within this burgeoning market [7], [8]

This study focuses on solar concentrator systems installed on predefined floor plans with possible physical obstructions. Each concentrator contains a prism-based internal structure composed of receiving prisms, which capture incident sunlight, and guiding prisms, which redirect light toward designated exits for energy harvesting. During this transmission process, optical losses may occur when light passes through air gaps between prism components, which directly affects system efficiency.

In practical applications, the performance of a solar concentrator system depends not only on the internal prism configuration of each unit but also on how the units are selected, arranged, and oriented within the available installation space. These decisions become more complex when the site includes obstructions, when exits may be embedded inside the concentrator, and when manufacturers are limited to a finite set of standardized concentrator types. Under such conditions, installation planning and internal prism design are strongly interdependent because site-level layout choices affect the feasible dimensions and operating conditions of each unit, while unit-level prism and exit configurations determine the resulting Total Light Efficiency (TLE) and economic return.

Previous studies have provided important insights into prism-based solar concentrator design and layout optimization. However, most existing works treat concentrator installation planning and internal prism design as separate problems. In addition, limited attention has been given to the simultaneous consideration of Blocklight obstructions, internal exits, standardized concentrator types, and economic trade-offs within a unified decision framework. This research gap is important because practical deployment requires these technical, spatial, and economic decisions to be made jointly rather than sequentially.

To address this gap, this study proposes a Bi-level Optimization Model for the integrated design and installation of solar concentrators. The upper level determines the selection, quantity, placement, and orientation of concentrators on the floor plan. The lower level optimizes the internal prism layout and exit configuration of each selected unit. A bi-level structure is required because the two decision levels are mutually dependent: the upper level defines the feasible installation context for each concentrator, whereas the lower level determines the TLE and exit-related cost information needed to evaluate the global installation plan. This integrated formulation enables the model to capture the interaction between spatial feasibility, optical performance, and economic profit more effectively than treating the two design tasks independently.

The main contributions of this study are as follows:

It formulates an integrated bi-level optimization model that jointly considers site-level solar concentrator installation and unit-level internal prism design.

It incorporates practical deployment constraints, including Blocklight obstructions, internal exits, standardized concentrator types, and profit-oriented decision criteria.

It provides a computational solution framework to generate feasible and economically effective solar concentrator configurations for constrained installation environments.

The remainder of this paper is organized as follows. Section 2 reviews the relevant literature. Section 3 presents the proposed bi-level mathematical model. Section 4 describes the solution approach. Section 5 reports the computational results and discussion. Section 6 concludes the paper and outlines future research directions.

2. Literature Review

2.1 Two-dimensional Spatial Layout Optimization

Kim and Moon [14] studied a two-dimensional shelf-space allocation problem in which rectangular products with specified widths and heights are selected and arranged under spatial and operational constraints. Regateiro et al. [15] developed a floor plan design approach based on block algebra and constraint satisfaction, in which topological and dimensional relations are used to generate feasible layout alternatives. Together, these studies show that two-dimensional layout optimization can be formulated by combining geometric feasibility constraints with higher-level selection and arrangement decisions.

These established theories provide the necessary basis for developing algorithms that maximize utilized area in glass sheet arrangements, ensuring complete non-overlapping coverage within predefined rectangular boundaries. By leveraging these constraint satisfaction and decomposition strategies, the proposed model can robustly handle geometric consistency and achieve high-

performance space efficiency objectives in solar concentrator installations.

2.2 Prism-Based Solar Concentrator Layout Design and Its Multiple-Objective Optimization

Wang et al. [11] proposed a genetic-algorithm approach for prism-based sunlight concentrator layout and reported that the optimized design improved light intensity by 55%. Wang and Yang [12] then developed a revised genetic algorithm that considered brightness, symmetry, reflection, and refraction, and their experiments reported brightness improvements exceeding 400% together with an 80% increase in symmetry. In addition, Wang and Dao [10] extended this research direction toward a multi-objective optimization setting that considered the trade-off between optical performance and economic return. Their study also reported improvements of 37.32% in light intensity and 34.56% in profit, providing a more practical decision framework for concentrator layout design.

In these prior works, authors typically considered exits to be located on the external boundaries of the concentrator, focusing primarily on increasing the quantity of exits rather than optimizing their specific spatial placement. In contrast, this study assumes that exits can be strategically installed within the interior of the solar concentrator to further enhance light harvesting efficiency. Additionally, instead of treating thickness as a continuous variable, we provide a predefined set of thickness options, allowing the mathematical model to select the most suitable dimensions for constructing and installing solar concentrator systems, as detailed in Section 2.7.

2.3 Snell's Law-based Light Guiding

This study presents a methodology for the design and installation of solar concentrator systems, which utilize assemblies of prisms as described in Table 2, consistent with previous research. Light propagation within these prism systems must comply with Snell's Law [13]. Mathematically, the interaction between light and the interface of two media is established based on the product of the absolute refractive index and the sine of the corresponding angle of transmission:

$$n_1 \times \sin\theta_1 = n_2 \times \sin\theta_2$$

where n_1 and n_2 represent the refractive indices of the incident and refractive media, respectively; while θ_1 and θ_2 denote the angles formed between the light ray and the surface normal. In the context of design optimization, such as for solar concentrators, this equation serves not only as a physical description but also as a core mathematical constraint. Solving the prism geometry optimization problem is essentially a process of adjusting parameters within Snell's Law to control energy trajectories, ensuring that radiation rays are accurately converged onto the absorbing surface with minimal error.

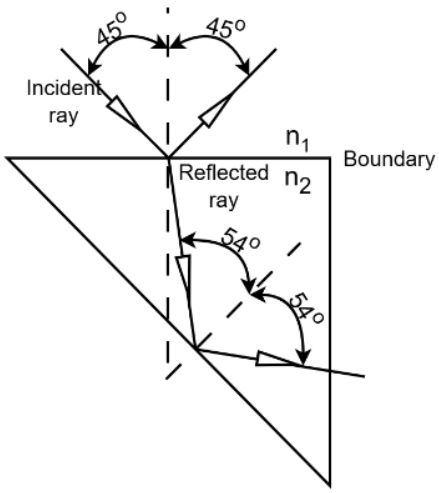


Figure 1. Light propagation across interfaces based on Snell's Law

2.4 Incident Angle and Light Propagation within Prisms

In practical applications, solar radiation does not always strike the surface vertically because the sun position changes throughout the day. Wang and Dao [10] indicated that incident angles from 45° to 135° can yield favorable optical efficiency, whereas vertical incidence at 90° produces the best performance. Based on the findings of Wang and Dao [10] and Wang et al. [11], the present study adopts a 90° incident angle as the controlled baseline condition for optimization.

Furthermore, as introduced previously, the solar concentrator system comprises two primary functional prism components: receiving prisms and guiding prisms. The receiving prisms are responsible for capturing incident sunlight from the external environment and directing it toward subsequent components. Conversely, the guiding prisms, which do not capture sunlight directly, serve to guide the light from the receiving units to the designated exits. This study assumes that when sunlight enters a receiving prism vertically (90° incident angle), it is propagated in four principal directions: Backward, Forward, Left, and Right. Within this framework, Snell's Law is applied to govern the light behavior and trajectories as discussed in the preceding sections.

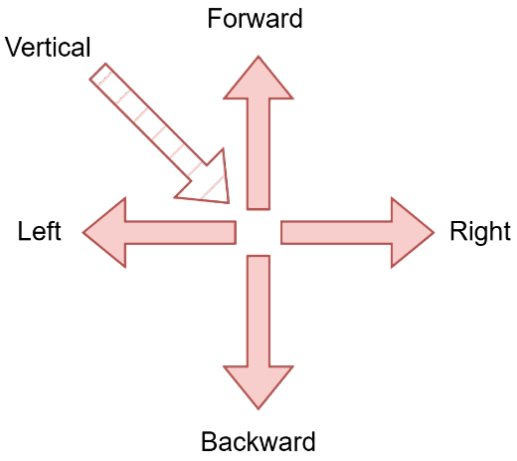


Figure 2. Light ray directions

2.5 Light Transmission Loss via Air Gaps

In this study, solar concentrator systems operate on the principle that solar energy is captured by receiving prisms and subsequently transported by guiding prisms to designated exits for energy conversion. While guiding prisms are exposed to sunlight, their vertical light collection efficiency is zero, as their primary function is the lateral redirection of light rather than direct vertical capture. The specific input and output directions for each prism type are detailed in Table 2. During the transmission of light from one prism to another, the beam may traverse air-filled regions, leading to a significant reduction in light efficiency due to reflection and attenuation between the optical interfaces.

This phenomenon is illustrated in detail in Figure 3. As light propagates according to Snell's Law - discussed in Section 2.3 - each instance of reflection or transition into an adjacent prism that involves an air gap results in a decrease in overall optical efficiency. This transmission loss is governed by the following formula:

$$Light\ transmission\ lost\ \% = \frac{r_1 - r_2}{r_1} \times 100$$
$$= 100 - \frac{r_2}{r_1} \times 100 = 100 - LTR$$

where the light transmission rate $(LTR) = (r_2/r_1) \times 100$. r_2, r_1 are the light efficiency received by prisms 1 and 2, respectively.

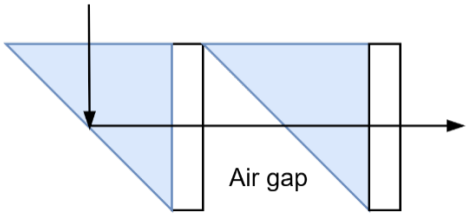


Figure 3. Light gaps between prisms during transmission

2.6 Issues of Internal Exit Quantities within Prisms

A primary objective in solar concentrator modeling is to achieve a strategic balance between the light harvesting efficiency delivered to the user and the manufacturing costs incurred by the enterprise. From the user's perspective, the performance is measured by the Total Light Efficiency (TLE), which represents the aggregate light intensity successfully transmitted from the receiving prisms to the exits. This transmission process is subject to optical losses whenever light traverses air gaps between prism components, as defined by the following formula derived from previous literature.

The individual optical efficiency at a given exit, denoted as I_F, can be formulated as a function of the cumulative attenuation experienced by the sunbeam along its trajectory. Specifically, the initial efficiency $I\big(x(i,j)\big)$ of a ray entering a prism at coordinates (i,j) is diminished by the transmission losses incurred at each interface. This relationship is expressed as follows:

$$I_F = I(x(i,j)LTR^A)$$

In this model, LTR represents the characteristic light transmission rate of the system, while the exponent accounts for the total number of air-filled gaps the light traverses before reaching the designated exit point.

Wang and Dao [10] demonstrated that increasing the number of exits in a solar concentrator significantly enhances overall light efficiency; however, it also leads to a substantial rise in production expenses due to the costs associated with each exit. While that model succeeded in identifying an optimal number of exits, those exits were typically restricted to the concentrator's periphery. In this research, we investigate whether strategically installing light exits within the internal grid of the concentrator - rather than only along its outer edges-can further enhance light harvesting and ultimately increase net profit. Our findings validate the feasibility and superior performance of integrating these internal exits within the solar concentrator units.

2.7 Issues Regarding Concentrator Types and Blocklight Obstructions

Wang and Dao [10] showed that utilizing larger concentrator dimensions - such as 10×13 instead of 10×11 - in conjunction with an increased number of exits can significantly enhance Total Light Efficiency (TLE) and achieve a more balanced profit margin between customers and manufacturers. Building upon these findings, the present study assumes a finite set of standardized, mass-produced concentrator types as model inputs. This allows the optimization framework to determine which specific concentrator dimensions should be selected and how the internal layout of each chosen unit should be meticulously designed. Specifically, five functional concentrator types with distinct dimensions are assumed for the installation: $10 \times 11;\ 10 \times 12;\ 10 \times 13;\ 10 \times 14;\ 10 \times 15$.

Furthermore, in practical installation scenarios, physical obstructions are inevitable. In this study, these are referred to as Blocklights, which represent restricted areas that prevent both the reception and transmission of sunlight. Within these designated Blocklight regions, neither prisms nor light exits can be installed. Our proposed model incorporates these obstructed zones within the floor plan to evaluate how the concentrator's design can be optimized. Regardless of the presence of these Blocklights, the model maintains its core objective - consistent with previous literature - of maximizing net profit to balance the conflicting interests of the energy user and the manufacturer [15].

Table 1. Comparison of modeling features in solar concentrator layout optimization studies

References	Optimization of solar concentrator layout	Considers change of concentrator size/thickness	Considers internal exits	Considers Blocklight /obstruction	Integrates floor-plan layout and internal prism design	Includes economic objective
Wang et al. (2014) – Prism-based Sunlight Concentrator Layout (PLGA)	x					
Wang & Dao (2020) – Multiple-objective optimization for solar concentrator layout	x	x				x
Current research (EAI)	x	x	x	x	x	x

Table 1 illustrates how solar concentrator optimization has evolved. While Wang et al. (2014) optimized internal layouts for fixed footprints, Wang and Dao (2020) incorporated dimensional variations and economic goals. Despite these advances, existing models treat structural decisions in isolation, overlooking the strict mathematical interdependence between macro-scale spatial allocation (floor plans with obstructions) and micro-scale optical routing (internal prisms with embedded exits).

This study addresses this gap through a unified bi-level framework that resolves these nested geometric and ray-tracing constraints simultaneously. The nested GA-GA architecture is not proposed as a novel mathematical algorithm variant; rather, it serves as a necessary

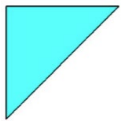
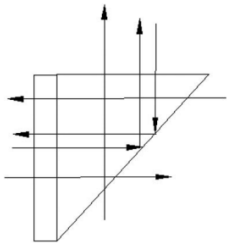
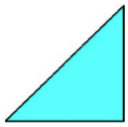
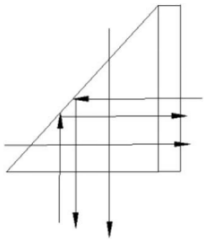
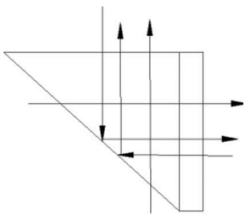
mechanism to decouple and jointly optimize the hierarchical layout dependencies.

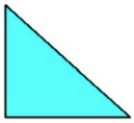
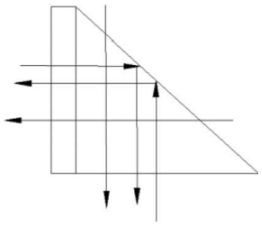
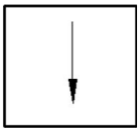
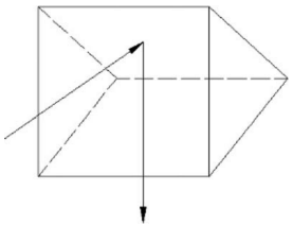
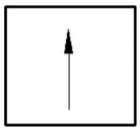
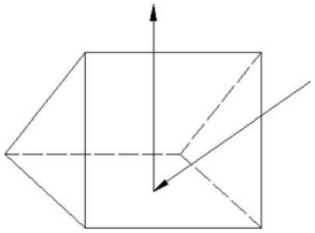
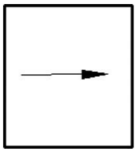
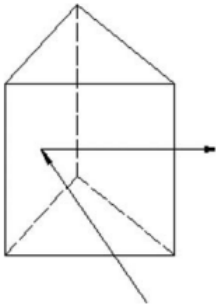
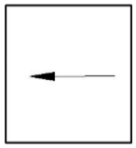
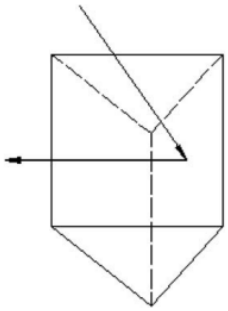
3. Modeling of Optimal Solar Concentrator Installation and Prism Layout Design

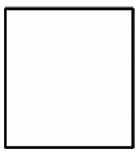
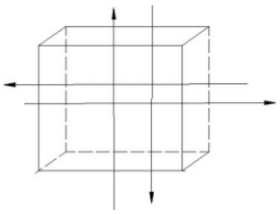
3.1. Problem statement

This study considers the design and installation of a prism-based solar concentrator system on a predefined floor plan with possible Blocklight obstructions. The objective is to determine the optimal concentrator types, installation coordinates, and internal prism configurations so as to maximize harvested light efficiency and total system profit. The proposed formulation is bi-level. At the upper level, the model determines which concentrators are activated, where they are placed, and whether they are rotated. At the lower level, the model determines the prism type assigned to each internal grid cell and the corresponding light-exit configuration for each installed concentrator. Within this framework, the incident angle of solar radiation is fixed at 90°, the Light Transmission Rate (LTR) between prisms is assumed constant, and the propagation of light through exits is restricted to a fixed direction. In addition, the model considers five standardized concentrator types with predefined dimensions as candidate installation units. Table 2 presents the light propagation rules and directional mapping of the prism types used in the model.

Table 2. Light Propagation Rules and Directional Mapping within Prisms

Prism	Type	Symbol	Visual performance	Direction in	Direction out
Guiding fiber	1			- Forward - Backward - Left - Right - Vertical	- Forward - Left - Left - Forward - Lost
	2			- Forward - Backward - Left - Right - Vertical	- Right - Backward - Backward - Right - Lost
	3			- Forward - Backward - Left - Right - Vertical	- Forward - Right - Forward - Right - Lost

	4			- Forward - Backward - Left - Right - Vertical	- Left - Backward - Left - Backward - Lost
Receiver fiber	5			- Forward - Backward - Left - Right - Vertical	- Lost - Lost - Lost - Lost - Backward
	6			- Forward - Backward - Left - Right - Vertical	- Lost - Lost - Lost - Lost - Forward
	7			- Forward - Backward - Left - Right - Vertical	- Lost - Lost - Lost - Lost - Right
	8			- Forward - Backward - Left - Right - Vertical	- Lost - Lost - Lost - Lost - Left

Path	9			- Forward - Backward - Left - Right - Vertical	- Forward - Backward - Left - Right - Lost

3.2 Assumptions and Limitations

The proposed bi-level model operates under three core constraints.

Fixed 90° incident angle. The solar incident angle is fixed at 90° as a controlled baseline condition. This assumption simplifies the ray-tracing procedure and allows the model to focus on the integrated design decisions of concentrator selection, floor-plan placement, internal prism configuration, and light-exit placement. In practice, the incident angle varies with time, season, and location; therefore, the reported results represent performance under the baseline condition rather than the annual performance of a real installation.

Constant Light Transmission Rate (LTR), treating LTR as constant assumes uniform optical materials and a clean environment. In practice, real-world degradation—such as dust fouling or thermal expansion at air gaps—would lower efficiency over time, requiring periodic maintenance to sustain the projected profit margins.

Static Blocklights. Blocklights are modeled as fixed obstruction regions representing permanent site constraints, such as structural elements, fixed equipment, or unavailable installation areas. This assumption allows the model to optimize concentrator placement and internal prism layouts under a stable obstruction pattern. However, it does not account for moving shadows caused by changing solar positions, nearby buildings, vegetation, or temporary objects.

Linear cost structure. The economic model assumes a constant area-based concentrator cost C_c and a constant setup cost C_E for each light exit. This simplified cost structure is adopted to provide a transparent baseline and to isolate the effects of concentrator selection, floor-plan placement, internal prism configuration, and light-exit placement on net profit. In practice, unit costs may vary with production volume because of material discounts, shared tooling, setup consolidation, and learning effects. These volume-dependent effects are not included in the present model.

Focusing on steady-state optimization ensures computational feasibility. Expanding the framework to handle dynamic, time-varying operational environments remains a target for subsequent iterations.

3.3 Set of indices

The set of indices used in the mathematical formulation is given in Table 3.

Table 3. Set of indices

Set / Index	Definition
$a \in \{1,2,3,\dots,n\}$	Index of solar concentrator.
$b \in B$	Index of Blocklight obstructions on the floor plan.
i, j	Grid-cell coordinates on the floor plan or within a concentrator.
$k \in \{1,2,3,4\}$	Index of the cell edges where light exits can be established.

3.4 Parameters

The parameters used in the model are summarized in Table 4.

Table 4. Set of parameters

Parameter	Definition
M, N	Dimensions (length and width) of the floor plan.
w_b, h_b	Width and height of Blocklight b.
i_b, j_b	Corner coordinates of Blocklight b.
b_a	Set of grid cells (i, j) within concentrator a occupied by a Blocklight zone.

w_{t_a}, h_{t_a}	Standard dimensions of concentrator type t_a before rotation.
C_c	Installation cost per unit area of a concentrator.
P	Revenue per unit of harvested TLE.
C_E	Setup cost per light exit.
D	Total customer demand for light efficiency.
U	Maximum allowable number of light exits per concentrator.

3.5 Set of variables

The variables used in the proposed bi-level formulation are classified into three groups: upper-level decision variables, lower-level decision variables, and a third group containing auxiliary variables together with the lower-level output variables. The first two groups represent the primary decisions made at each level. The third group contains variables used to express geometric relationships, obstruction mapping, and the information returned from the lower level to the upper level. In particular, TLE_a and E_a are generated by the lower-level formulation and then passed to the upper-level formulation for profit evaluation.
The variables of the bi-level model are listed in Table 5, Table 6 and Table 7.

Table 5. Set of upper-level decision variables

Variable	Definition
$z_a \in \{0,1\}$	Equals 1 if concentrator a is activated, and 0 otherwise.
$r_a \in \{0,1\}$	Rotation status of concentrator a, where 0 denotes no rotation and 1 denotes a 90° rotation.
t_a	Selected concentrator type from the standardized set.
i_a, j_a	Installation coordinates of concentrator a on the floor plan.

Table 6. Set of lower-level decision variables

Variable	**Definition**
$x(i,j)$	Prism type assigned to cell (i,j) within the concentrator.
$e(i,j,k) \in \{0,1\}$	Equals 1 if a light exit is established on edge k of cell (i,j), and 0 otherwise.

Table 7. Auxiliary variables and lower-level output variables

Variable	Role	Definition
$w^*_{t_a}, h^*_{t_a}$	Auxiliary variables	Actual dimensions of concentrator a after rotation.
$u_{ab} \in \{0,1\}$	Auxiliary variable	Indicates whether concentrator a intersects Blocklight b.
i'_{ab}, j'_{ab}	Auxiliary variables	Local coordinates of Blocklight b within concentrator a.
w'_{ab}, h'_{ab}	Auxiliary variables	Local width and height of the obstructed region within concentrator a.
TLE_a	Lower-level output variable	Total Light Efficiency of concentrator a, computed by the lower-level formulation and returned to the upper level.
E_a	Lower-level output variable	Total number of light exits of concentrator a, computed by the lower-level formulation and returned to the upper level.

3.6. Objective Functions

The proposed bi-level mathematical model addresses the integrated problem of spatial installation and detailed structural design for solar concentrators as follows. At the Upper Level (Level 1), the model focuses on the optimal arrangement of concentrators on the floor plan, with the objective of maximizing net profit after deducting the installation and utilization costs of the selected concentrators. The configuration of the activated concentrators is then passed down to the Lower Level (Level 2). At this stage, the model determines the internal layout for each specific concentrator, calculating the profit derived from the harvested light efficiency (TLE) minus the costs associated with establishing the light exits. Consequently, the objective of the lower level is also to maximize this localized profit. The formal mathematical formulation is presented below.

3.6.1 Upper-Level

Level 1 decides on concentrator selection and spatial installation on the floor plan, based on installation costs and the resulting returns. The objective is to maximize the total net profit, calculated as the aggregate revenue generated by all utilized concentrators $\sum_{a=1}^{n} TLE_a \times P$ minus their respective installation costs on the site $\sum_{a=1}^{n} -(z_a \times {w^*}_{t_a} \times {h^*}_{t_a}) \times C_c + E_a \times C_E$.

Maximize:

$$\sum_{a=1}^{n} -(z_a \times {w^*}_{t_a} \times {h^*}_{t_a}) \times C_c + TLE_a \times P - E_a \times C_E \ (1)$$

Subject to:

For clarity, the upper-level constraints are grouped into four functions: rotation and effective dimensions, floor-plan feasibility, Blocklight localization, and demand control.

Rotation and effective dimensions:

$${w^*}_{t_a} = (1 - r_a) \times w_{t_a} + r_a \times h_{t_a} \ \forall a \in \{0,1,2,\dots,n\} \ (2)$$

$${h^*}_{t_a} = (1 - r_a) \times h_{t_a} + r_a \times w_{t_a} \ \forall a \in \{0,1,2,\dots,n\} \ (3)$$

Constraints (2) and (3) determine the actual width and height of concentrator a after rotation. These constraints connect the selected type t_a with the binary rotation variable r_a, so the model always uses the correct footprint in subsequent placement decisions. When $r_a = 0$, the concentrator keeps its original dimensions (w_{t_a}, h_{t_a}). When $r_a = 1$, the two dimensions are exchanged, which represents a 90° rotation. This formulation accounts for orientation-driven changes in the occupied area, which directly influence boundary feasibility and obstruction mapping.

Floor-plan feasibility:

$$0 \le i_a \le M - {w^*}_{t_a} \ \forall a \in \{0,1,2,\dots,n\} \ (4)$$

$$0 \le j_a \le N - {h^*}_{t_a} \ \forall a \in \{0,1,2,\dots,n\} \ (5)$$

Constraints (4) and (5) ensure that each installed concentrator remains within the $A \times B$ floor plan. Constraint (4) limits the horizontal coordinate i_a by the effective width $w^*_{t_a}$, while Constraint (5) limits the vertical coordinate j_a by the effective height $h^*_{t_a}$. Together, these constraints prevent any part of a concentrator from extending beyond the admissible installation area.

Blocklight localization:

$$z_a = 1 \, ; z_{a'} = 1 \Rightarrow (i_a + {w^*}_{t_a} \le i_{a'}) \vee (i_{a'} + {w^*}_{t_a} \le i_a) \vee (j_a + {h^*}_{t_a} \le j_{a'}) \vee (j_{a'} + {h^*}_{t_a} \le j_a) \ \forall a, a' \in \{0,1,2,\dots,n\}; a \ne a' \ (6)$$

$$u_{ab} = 1 \Leftrightarrow \min(i_a + {w^*}_{t_a}, i_b + w_b) > \max(i_a, i_b) \wedge \min(j_a + {h^*}_{t_a}, j_b + h_b) > \max(j_a, j_b) \ \forall a \in \{0,1,2,\dots,n\}; \forall b \in B \ (7)$$

$$u_{ab} = 1 \Rightarrow {i'}_{ab} = \max(0, i_b - i_a) \ \forall a \in \{0,1,2,\dots,n\}; \forall b \in B \ (8)$$

$$u_{ab} = 1 \Rightarrow {j'}_{ab} = \max(0, j_b - j_a) \ \forall a \in \{0,1,2,\dots,n\}; \forall b \in B \ (9)$$

$$u_{ab} = 1 \Rightarrow {w'}_{ab} = \min(i_a + {w^*}_{t_a}, i_b + w_b) - \max(i_a, i_b) \ \forall a \in \{0,\dots,n\}; \forall b \in B \ (10)$$

$$u_{ab} = 1 \Rightarrow {h'}_{ab} = \min(j_a + {h^*}_{t_a}, j_b + h_b) - \max(j_a, j_b) \ \forall a \in \{0,\dots,n\}; \forall b \in B \ (11)$$

$${w'}_{ab} \le 0 \vee {h'}_{ab} \le 0 \Longrightarrow u_{ab} = 0 \ \forall a \in \{0,1,2,\dots,n\}; \forall b \in B \ (12)$$

Constraint (7) identifies whether concentrator a intersects Blocklight b. It compares the horizontal and vertical intervals of the concentrator and the obstruction on the global floor plan. If both intervals overlap, the binary variable u_{ab} is activated, indicating that Blocklight b affects concentrator a. Constraints (8) and (9) transform the global coordinates of the obstruction into local coordinates within concentrator a. These constraints determine where the obstructed region begins relative to the local grid of that concentrator. Constraints (10) and (11) compute the local width and height of the overlapped Blocklight region. Only this overlapped portion is relevant to the lower-level design. Constraint (12) removes degenerate cases by forcing $u_{ab} = 0$ whenever the computed overlap has non-positive width or height. This prevents invalid obstruction regions from being transferred to the lower level.

Demand control:

$$\sum_{a=1}^{n} TLE_a \le D \ (13)$$

Constraint (13) limits the total TLE delivered by all concentrators so that the system does not exceed the customer demand D. This constraint keeps the installation plan aligned with the required output and avoids selecting unnecessary capacity once the demand has been met.

3.6.2 Lower-Level

Level 2 decides on the detailed internal configuration of prisms within the solar concentrator. The objective is to maximize the localized profit, which is determined by the revenue generated from the Total Light Efficiency $TLE(x(i,j), e(i,j,k)) \times P$ minus the costs incurred from establishing the light exits $C_E \times \sum_{i=1}^{w_a} \sum_{j=1}^{h_a} \sum_{k=1}^{4} e(i,j,k)$.

Maximize:

$$\sum_{i=1}^{w_a}\sum_{j=1}^{h_a} TLE\big(x(i,j),e(i,j,k)\big) \times P - C_E \times \sum_{i=1}^{w_a}\sum_{j=1}^{h_a}\sum_{k=1}^{4} e(i,j,k) \quad (14)$$

Subject to:

The lower-level constraints are grouped into three functions: performance aggregation, prism assignment feasibility, and light-exit feasibility**.**

Performance aggregation:

$$TLE_a = \sum_{i=1}^{w_a}\sum_{j=1}^{h_a} TLE\big(x(i,j),e(i,j,k)\big) \quad (15)$$

$$E_a = \sum_{i=1}^{w_a}\sum_{j=1}^{h_a}\sum_{k=1}^{4} e(i,j,k) \quad (16)$$

Equation (15) defines the Total Light Efficiency TLE_a of concentrator a as the aggregate light performance generated by the selected prism layout and light-exit configuration. This value is the main optical performance measure returned to the upper level. Equation (16) defines E_a as the total number of light exits established in concentrator a. This quantity is also returned to the upper level because each exit contributes to the total cost through the parameter C_E. Together, Equations (15) and (16) provide the information required to evaluate each installed concentrator at the upper level.

Prism assignment feasibility:

$$1 \le x(i,j) \le T \;\forall\, (i,j) \notin b_a, x(i,j)\ is\ integer \quad (17)$$

$$x(i,j) = 0 \;\forall\, (i,j) \in b_a \quad (18)$$

Constraint (17) requires each non-blocked cell (i,j) to be assigned a valid prism type. The variable $x(i,j)$ is restricted to integer values from 1 to T, where T denotes the number of prism types listed in Table 2. This means that every usable cell in the concentrator must contain one admissible prism component. Constraint (18) handles the Blocklight effect at the local level by forcing $x(i,j) = 0$ for every cell belonging to the blocked set b_a. As a result, no prism can be placed in a physically obstructed cell. This ensures that the internal design remains consistent with the local geometry inherited from the upper level.

Light-exit feasibility:

$$e(i,j,k) = \{0;1\} \quad (19)$$

$$1 \le E_a \le U \quad (20)$$

$$e(i,j,k) = 0 \;\forall\, (i,j) \in b_a \quad (21)$$

Constraint (19) defines $e(i,j,k)$ as a binary variable, indicating whether a light exit is established on edge k of cell (i,j). This model exit placement as a discrete structural decision. Constraint (20) limits the total number of exits in concentrator a by the allowable upper bound U. This reflects a practical trade-off, because additional exits may improve light harvesting but also increase structural complexity and manufacturing cost. Constraint (21) prohibits light-exit placement in Blocklight cells by forcing $e(i,j,k) = 0$ whenever $(i,j) \in b_a$. This prevents infeasible designs in which exits are assigned to obstructed cells.

4. Solution Approach

4.1 Genetic Algorithm for Concentrator Installation on the Floor Plan

At the first level, the solution approach focuses on combinatorial optimization and the bin-packing problem applied to the designated floor plan. The process begins with the encoding and initialization stage, where each individual in the population represents a potential layout configuration. Each chromosome consists of genes determining the concentrator type t_a, activation status z_a, rotation angle r_a, and a priority value for placement. To transform these genotypes into physical coordinates (i_a, j_a), a decoder based on the First-Fit strategy is implemented. The algorithm scans the floor area $M \times N$ to identify the first available position that is not occupied by fixed obstructions (Blocklights) or previously placed concentrators, following the encoded priority sequence.

Once a position is determined, the system performs a geometric intersection calculation between the global Blocklights and the boundaries of each concentrator to establish an "internal Blocklight" matrix. The normalized information regarding the dimensions and coordinates of these obstructed regions is then transferred to Level 2 to serve as boundary conditions for the optical performance evaluation. Finally, Level 1 executes evolutionary operators, such as two-point crossover and mutation, on the concentrator identification genes to refine the floor configuration across generations. The ultimate goal is to maximize the effective light-harvesting area while ensuring the total output does not exceed the system's actual Demand D.

4.2 Proposed Genetic Algorithm for Prism Layout Optimization

Level 2 operates independently for each concentrator configuration received from Level 1, focusing on optimizing the prism arrangement matrix and the strategic placement of light exits. The algorithm employs an evolutionary cycle consisting of selection, crossover, and mutation to refine the internal design. Following Wang and Dao [10], the selection stage gives priority to layouts with

higher Total Light Efficiency (TLE) after accounting for exit-establishment costs. This is followed by a crossover process, which facilitates the exchange of prism configurations and guiding patterns between parent layouts to produce superior offspring. Furthermore, mutation operators are applied to introduce random adjustments to both the prism types and their specific exit locations within the grid. Once the optimization process reaches convergence, the resulting TLE and the associated exit installation costs for each concentrator are transmitted back to Level 1, providing the essential fitness data required for the upper-level evaluation of the global floor plan.

Table 8. Model Parameter

Parameter	Value
P	100
C_c	300
C_E	3000
LTR	80%

4.3 Proposed Genetic Algorithm for Solar Concentrator Installation and Prism Layout Optimization

To maximize net profit under a complex system of physical and spatial constraints, this problem uses a nested evolutionary mechanism with two distinct Genetic Algorithm (GA) levels. GA is selected for this bi-level formulation because the interaction between macro-scale layout planning and micro-scale optical routing yields a discontinuous, non-differentiable, and highly combinatorial search space. Traditional gradient-based optimization cannot handle these discrete variables and sharp geometric constraints (such as Blocklights). The population-based nature of GAs aligns with this hierarchical structure, enabling Level 1 to explore global layouts while triggering parallel lower-level evaluations for each candidate solution.

This structure synchronizes global concentrator placement on the floor plan with detailed internal prism design, creating an integrated multi-level optimization process. The coordination forms a closed-loop system that ensures data integration and search efficiency. During each generational cycle, Level 1 runs Level 2 in parallel for all population candidates. The resulting Total Light Efficiency (TLE) and localized performance data are aggregated into a net profit value, which serves as the upper-level fitness score. Synchronized iterations repeat until satisfying a predefined stopping criterion, such as maximum generations or steady-state profit convergence (refer to Figure 4 for further details).

To reduce redundant lower-level evaluations, a caching mechanism is implemented in the Level-2 optimization procedure. During the upper-level search, different candidate solutions may generate identical panel configurations after decoding. A cache key is created from the panel dimensions, rotation status, and local Blocklight configuration.

Before executing the Level-2 Genetic Algorithm, the algorithm checks whether the corresponding cache key has been evaluated previously. If a cache hit occurs, the stored Total Light Efficiency (TLE), exit cost, prism-layout matrix, and exit-layout matrix are retrieved directly. If a cache miss occurs, the Level-2 Genetic Algorithm is executed and the resulting values are stored in the cache for subsequent reuse.

Because cached results are retrieved only for identical lower-level configurations, the caching mechanism does not modify the objective function, constraints, or feasible solution space. Its purpose is to avoid repeated optimization of equivalent subproblems and reduce computational time.

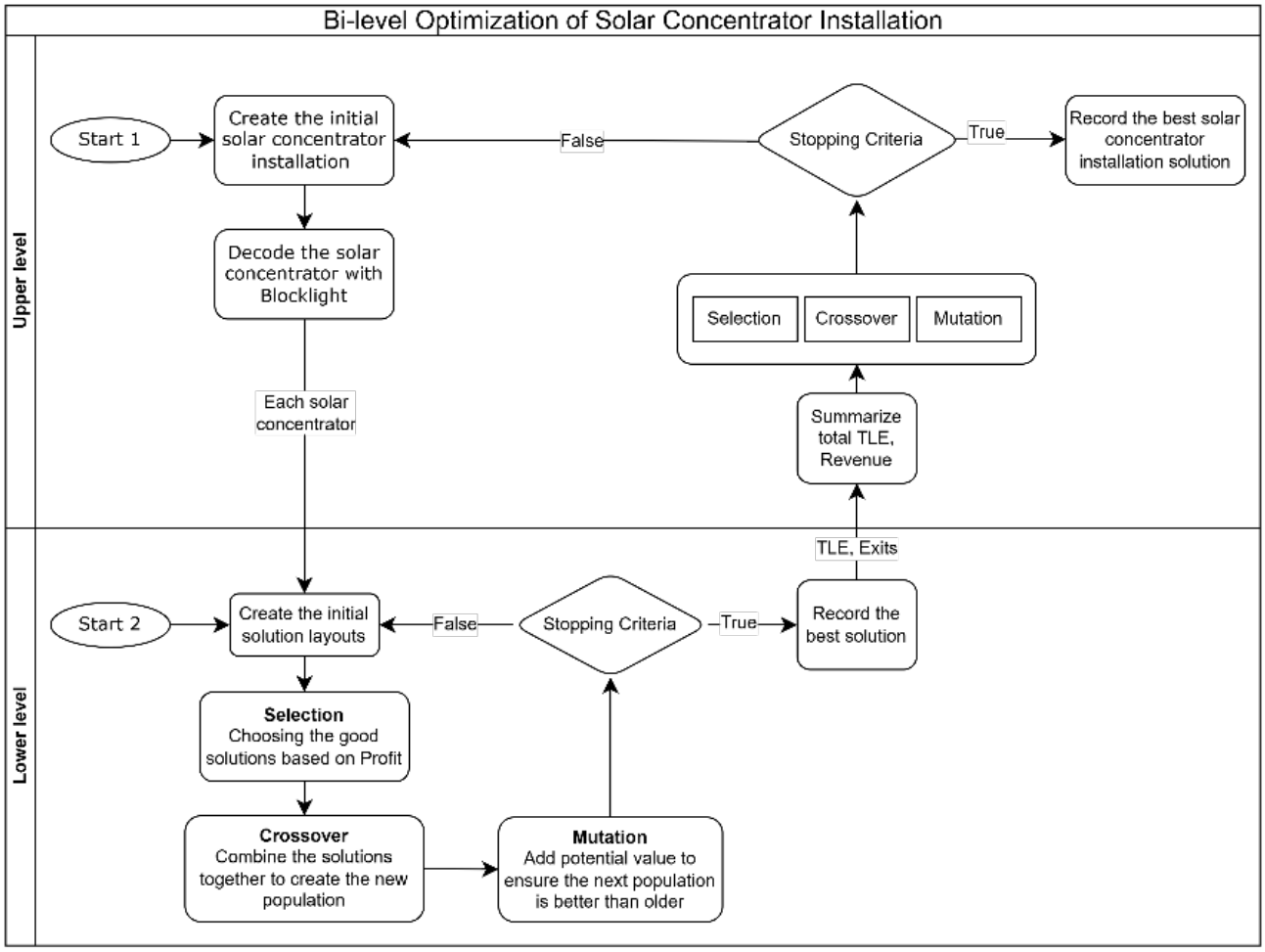


Figure 4. GA-based computational procedure for bi-level optimize solar concentrator installation

5. Experiment

This study proposes an optimized internal prism configuration for solar concentrator systems, specifically featuring light exits integrated within the concentrators' interior. On a macro scale, the research presents a mathematical model designed to optimize the installation of these solar concentrators across a floor plan, accounting for various scenarios involving different obstruction placements. To address this hierarchical problem, the solution methodology first employs a Genetic Algorithm (GA) at the Lower Level to refine the internal layout and internal exit positioning for each concentrator. Subsequently, an UpperLevel GA is implemented to determine the optimal global installation of the concentrators on the floor plan. The specific operational mechanisms of these algorithms, as detailed in Sections 4.1 and 4.2, are validated through the experimental results presented in the following subsections. All experiments were conducted on a laptop equipped with an Intel Core i7 processor and 32GB of RAM. The algorithms were implemented in Python using the Visual Studio Code (VS Code) with the DEAP framework for evolutionary computation, while Numba was used to improve computational efficiency [19-24]. Their performance is evaluated in the experimental results presented in the following subsections.

5.1. Optimization of Solar Concentrator Installation on the Floor Plan

Experiment 1 was conducted using a designated floor plan with dimensions $M = 20$ and $N = 32$, representing its height and width, respectively. The layout includes a fixed obstruction, designated as Blocklight, positioned at $(i_b, j_b) = (4, 6)$ with dimensions of $h_b = 4$, $w_b = 7$, as illustrated in Figure 6. Given a customer demand of $D = 22000\ luminous$, various concentrator types $t_a = \{1, 2, 3, 4, 5\}$ were allocated across the floor plan utilizing the proposed Genetic Algorithm (GA) with a population size of 300, 150 generations, a crossover rate of 0.8, and a

mutation rate of 0.2. The resulting optimal configuration is presented in Figure 6.

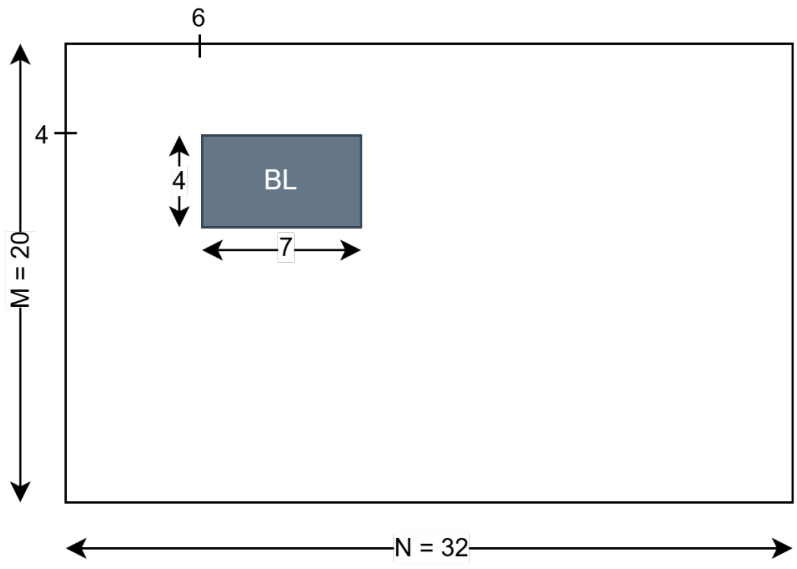


Figure 5. Floor plan in experiment 1

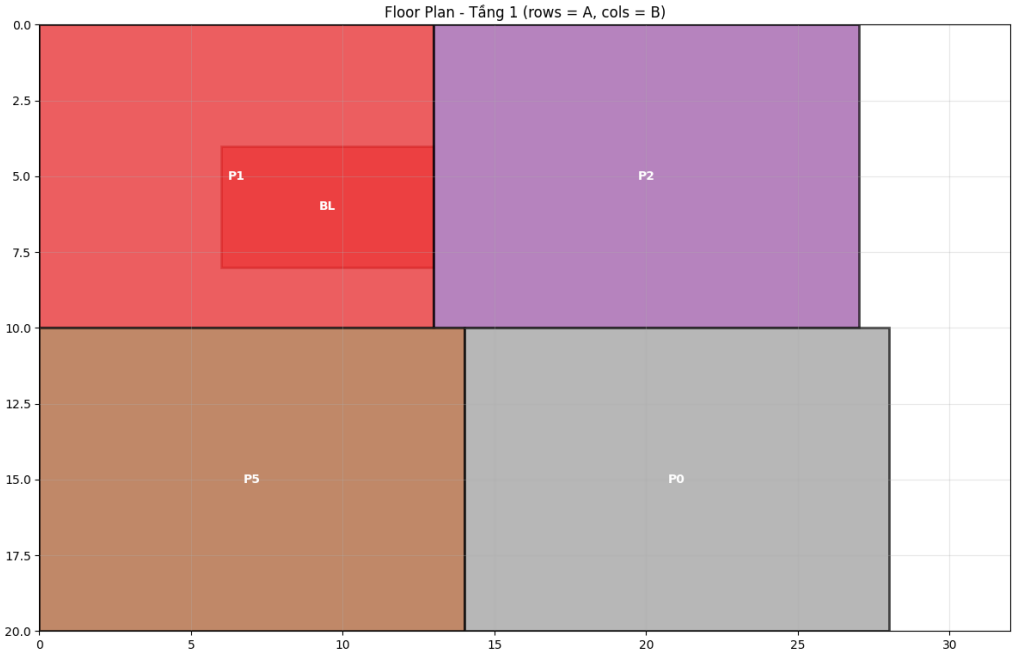


Figure 6. Result of solar concentrator installation in experiment 1

The obtained solution achieves a Total Light Efficiency (TLE) of 20,650.8 luminous, generating an effective revenue of 2,065,083.4 (capped by the demand constraint D). The total production and inventory costs amount to 345,000, encompassing both prism costs (C_c) and light exit

costs (C_E) for each concentrator, resulting in a final net profit of 1,720,083.4.

These experimental results demonstrate distinct engineering advantages over traditional isolated optimization approaches. The placement of Concentrator P1 over the Blocklight zone illustrates the framework's capacity to map global floor-plan obstructions into local matrix constraints. By translating these barriers into boundary conditions for the unit-level design, the lower-level solver exploits the remaining valid area of the panel rather than leaving the footprint vacant, thereby achieving high spatial efficiency without risking optical blockage. This geometric adaptability is complemented by high optical performance, as the achieved TLE tightly approaches the customer demand limit. Such results prove that embedding exits strategically within the internal prism grid successfully counters the cumulative attenuation typically caused by air gaps. From a financial perspective, the bi-level integration directly balances area-based installation costs C_C against fixed exits setup expenditures C_E, providing a quantitative decision-support tool for manufacturers to verify if hardware modifications are fully justified by marginal revenue returns.

Detailed specifications for each individual concentrator are presented in the following figures 7-10.

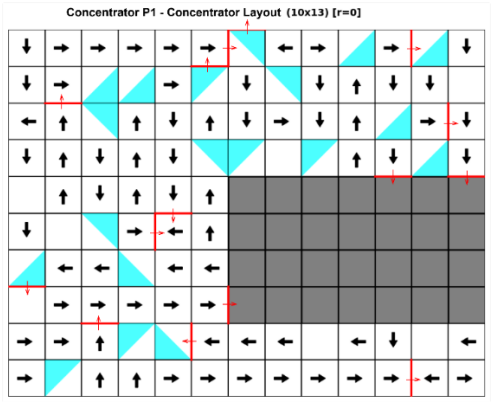


Figure 7. Concentrator 1 of Floor Plan (TLE = 4698.5, Profit = 385852)

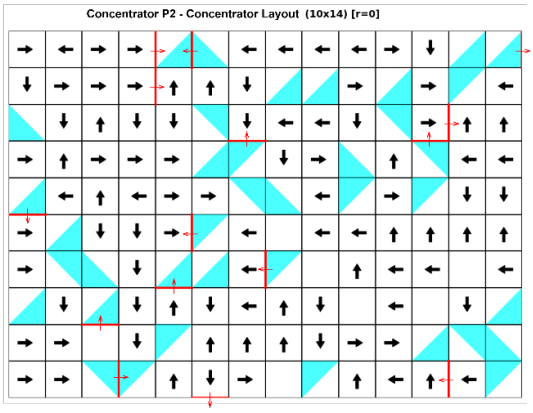


Figure 8. Concentrator 2 of Floor Plan (TLE = 5317.4, Profit = 444744)

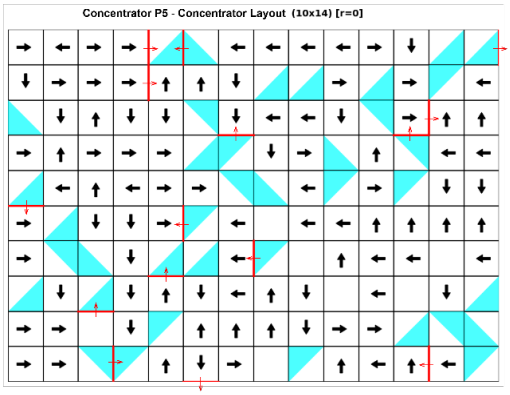


Figure 9. Concentrator 3 of Floor Plan (TLE = 5317.4, Profit = 444744)

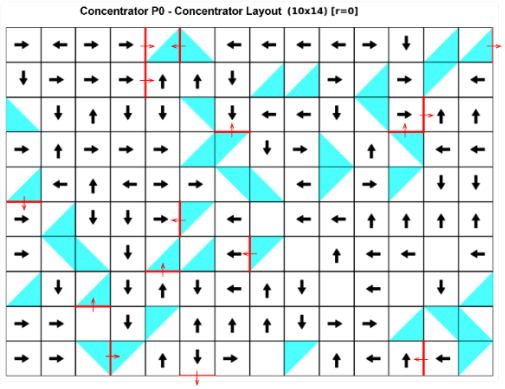


Figure 10. Concentrator 4 of Floor Plan (TLE = 5317.4, Profit = 444744)

5.2 Convergence analysis of the GA-GA Algorithm

The convergence behavior of the GA-GA algorithm is illustrated in Figure 11, which tracks the evolution of Best Fitness and Average Fitness across successive generations. The results indicate that the Best Fitness value increases rapidly during the initial stages and reaches a steady state after approximately 10 generations, suggesting that the algorithm effectively identifies high-quality solution regions at an early stage. Meanwhile, the Average Fitness continues to fluctuate throughout subsequent generations, reflecting the maintenance of population diversity during the search process. The early stabilization of the Best Fitness is partly attributed to the structural characteristics of the problem, where the number of feasible layout configurations on the installation floor plan is relatively limited. Consequently, diverse solutions within the search space may lead to layouts with equivalent objective values, thereby facilitating a relatively rapid convergence process.

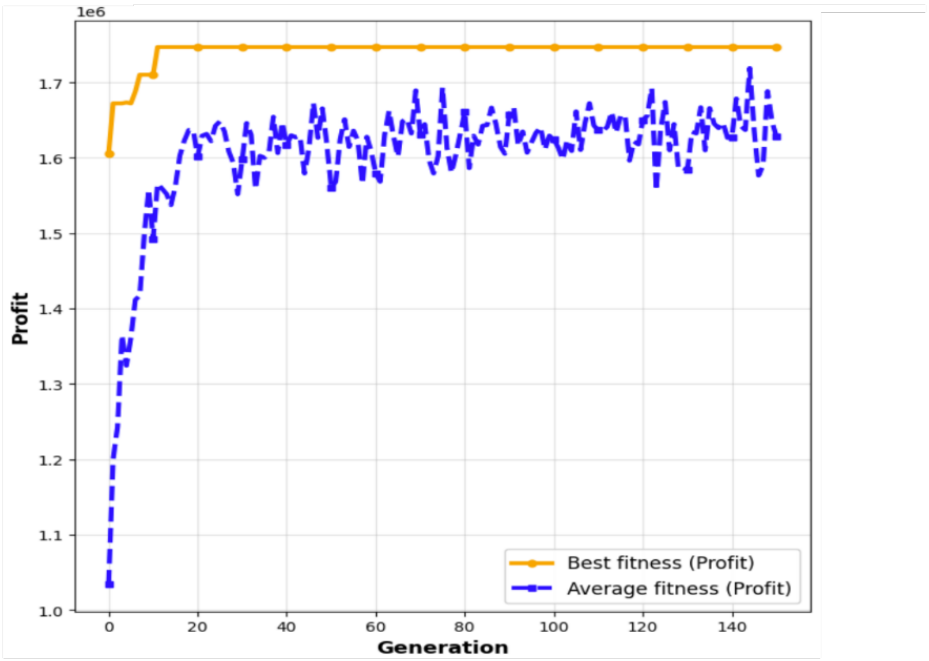


Figure 11. Evolution of best and average fitness in GA- GA

5.3 Effect of Lower-Level Algorithm Selection

To assess the sensitivity of the proposed bi-level framework to the choice of lower-level solver, three algorithm configurations were evaluated: GA-GA, GA-PSO, and GA-SA. In each configuration, a Genetic Algorithm (GA) was consistently employed at the upper level to determine the global concentrator layout, while the lower-level solver was varied as the sole experimental factor. All upper-level parameters were held constant - population size of 300, 150 generations, crossover rate of 0.8, and mutation rate of 0.2 - to ensure that performance differences were attributable exclusively to the lower-level algorithm.

Across all three implementations, a repair procedure was incorporated to correct infeasible exit configurations so that the number and placement of exits remained consistent with the admissible lower-level solution structure.

Table 9. Parameter settings for lower-level GA, SA, and PSO

Algorithm	Settings
Genetic Algorithm (GA)	Generations = 200

	Population size = 10,000
	Selection: tournament selection ($k = 3$)
	Crossover: two-point crossover ($p = 0.95$)
	Mutation rate = 0.05
	Elite preservation via Hall of Fame
Simulated Annealing (SA)	Initial temperature = 1000
	Final temperature = 0.01
	Cooling rate = 0.995
	Cooling schedule: geometric
	Iterations per temperature level = 50
	Neighborhood move: random gene perturbation with repair
Particle Swarm Optimization (PSO)	Stopping rule: $n_iter = 150$
	Swarm size = 100
	Inertia weight $w = 0.7$
	Cognitive coefficient $c_1 = 1.5$
	Social coefficient $c_2 = 1.5$
	Velocity limit $v_{max} = 2.0$
	Discrete mapping: rounding followed by repair

Across all three implementations, a repair procedure was incorporated to correct infeasible exit configurations so that the number and placement of exits remained consistent with the admissible lower-level solution structure.

The three lower-level approaches differ fundamentally in their search mechanisms. Holland [25] described Genetic Algorithms as search procedures that use selection, crossover, and mutation to maintain diversity and explore complex solution spaces. Zomaya and Kazman [26] and Kirkpatrick et al. [27] explained that Simulated Annealing can accept inferior solutions to escape local optima, although this mechanism is often less effective in dense discrete spaces. Kennedy and Eberhart [28] introduced Particle Swarm Optimization as a best-position update process that can converge quickly but may stagnate when diversity is lost.

Figure 12 shows the convergence trajectories of the three bi-level configurations. The GA-GA configuration attains the highest fitness value of 1,720,083.4 and stabilizes after approximately 10 generations. GA-PSO reaches 1,421,217.34 but plateaus at an intermediate level, whereas GA-SA yields the lowest fitness value, 656,631.03, and converges earlier to a suboptimal region. In terms of computational cost, GA-GA requires about 6 hours, GA-PSO about 1.5 hours, and GA-SA about 40 minutes.

The rapid stabilization of the GA-GA configuration within the first 10 generations appears to stem from structural features of the problem. In particular, the chromosome encoding and decoding procedure used in this study can map different chromosomes to effectively identical layout solutions, which reduces the diversity of meaningful upper-level candidates. Moreover, the limited dimensions of the floor plan further narrow the set of feasible placement patterns. Similar premature-convergence behavior in constrained genetic search has also been reported by Chen et al. [29] and Hassanat et al. [30].

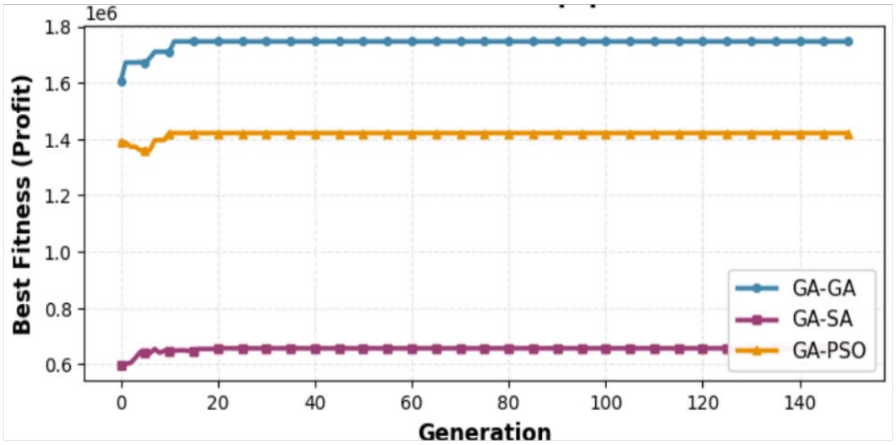


Figure 12. Fitness Evolution of GA-GA, GA-SA, and GA-PSO

Although the GA–GA configuration achieved the highest fitness value, its runtime of approximately 6 hours is a practical limitation of the current implementation. The main computational burden arises from the nested solution structure: each upper-level candidate layout requires lower-level optimization of the internal prism layout and light-exit positions for the selected concentrators. This burden is expected to increase for larger floor plans, more concentrator types, additional Blocklight regions, or repeated evaluations under different operating scenarios.

For the tested case, the runtime is acceptable because the proposed method is intended for offline installation planning rather than real-time operation. However, computational acceleration will be necessary for larger-scale applications. Possible improvements include caching repeated lower-level evaluations, parallel computation, and adaptive stopping criteria based on convergence behavior.

6. Conclusion

This research successfully develops a bi-level optimization model bridging macro-scale spatial layout planning and micro-scale optical engineering for prism-based solar concentrators. The primary contribution lies in the integrated mathematical formulation that couples site-level allocation with internal unit design under localized obstructions. Within this framework, the nested GA-GA architecture is deployed not as a standalone algorithmic novelty, but as a dedicated solution strategy required to decouple and jointly optimize these highly interdependent hierarchical layout decisions.

Level 1 coordinates the selection of standard concentrator types from a predefined catalog, establishing placement coordinates and rotation angles to maximize floor plan utilization while avoiding physical Blocklight obstructions. Simultaneously, Level 2 refines the internal structural layout by configuring the receiving and guiding prism matrix alongside internal light exits to maximize Total Light Efficiency (TLE). A core aspect of this work is the economic model integrating technical performance with financial metrics, including TLE-based revenue, area-based production costs, exit setup expenditures, and customer demand constraints. Python-based computational experiments demonstrate that this integrated GA-GA approach achieves a peak net profit of 1,720,083.4 currency units.

Despite these performance metrics, the current static framework presents distinct deployment limitations under real-world operating conditions. The assumption of a fixed 90° vertical light incidence establishes an idealized baseline but omits diurnal solar movement. Practical deployment without an active tracking mechanism would introduce time-varying angular variations, significantly degrading the actual accumulated TLE over a day. Similarly, treating the light transmission rate (LTR) as a constant ignores environmental factors such as dust fouling or thermal expansion at internal air gaps, which would reduce efficiency over time without periodic maintenance.

To address these limitations, future research will shift from steady-state optimization to dynamic environmental modeling. Key expansions will integrate machine learning for predictive shading and time-varying light tracking, alongside multi-objective optimization via NSGA-II to evaluate competing technical and financial criteria. Advancing to 3D multi-level configurations and expanding the optimization boundary to encompass factory-to-site supply chain logistics will further facilitate scalable, economically viable renewable energy deployments in modern smart cities.

Future work will also benchmark the proposed GA–GA framework against exact optimization models on reduced problem instances. Such a comparison would provide a

reference for evaluating solution quality and calculating the optimality gap. However, formulating the complete problem as a mixed-integer model is challenging because it combines discrete concentrator placement, prism assignment, internal light-exit decisions, Blocklight constraints, and path-dependent light propagation. In particular, the lower-level ray-tracing process includes direction changes, transmission losses, and loop-detection conditions. A CPLEX-based formulation for small benchmark instances is currently under development.

Declarations

Ethics approval and consent to participate

This article does not contain any studies with human participants or animals performed by any of the authors.

Availability of data and materials

All the data used have been presented in the manuscript and no additional source data are required.

Competing interests

All the authors declare that they have no conflict of interest.

Authors' contributions

Author Le Duc Dao develops ideas and writing while Nguyen Thanh Loi contribute to writing and coding.

Acknowledgements

We acknowledge Ho Chi Minh City University of Technology (HCMUT), VNU-HCM for supporting this study.

Appendix

TLE Calculation Procedure

Step 1: Generate a layout matrix x with dimensions corresponding to each concentrator type a.

Step 2: Generate an exit matrix e with dimensions corresponding to each concentrator type a.

Step 3: Initialize Total Light Efficiency $(TLE) = 0$.

Step 4: Calculate Total Light Efficiency (TLE)

For $i = 1$ to length w_a

For $j = 1$ to length h_a

If $x(i,j)$ is a guiding prism or a blocklight (indicated by values 1, 2, 3, 4, 9, or 0): Set individual efficiency $ef = 0\%$ and skip.

Otherwise, if $x(i,j)$ is a receiving prism (indicated by values 5, 6, 7, or 8), proceed to the following verification steps:

Check for Exit:

If a light ray from $x(i,j)$ propagates in direction k and an exit is present $e(i,j,k) = 1$: Update $ef = 1$ and include it in the Total Light Efficiency (TLE).

Conversely, if the light ray from $x(i,j)$ in direction k does not encounter an exit $e(i,j,k) = 0$: Proceed to update the light's position and orientation to simulate its optical trajectory. At the new coordinates, evaluate the following criteria:

Blocklight Verification: Examine the propagation path for obstructions; if the light ray enters a Blocklight zone, the path is terminated and ef is set to 0.

Air Gap Verification: Track the air-filled spaces traversed by the beam.

Loop Verification: Monitor for internal reflection loops within the configuration.

A loop occurs when light is reflected back to a previously visited position in the same direction, failing to reach an exit. In such instances, ef is assigned a value of zero.

Exit Detection: If the ray successfully reaches a light exit without encountering a loop, update ef by applying the LTR attenuation formula and aggregate the result into the TLE.

End for w_a

End for h_a

Step 5: Final TLE Aggregation

The TLE is defined as the sum of the current light efficiencies (ef) at all exits:

$$TLE = SUM\ (ef)$$

Step 6: Calculate the net profit based on the established formula.

$$\sum_{i=1}^{w_a}\sum_{j=1}^{h_a} TLE(x(i,j), e(i,j,k)) \times P - C_E \times \sum_{i=1}^{w_a}\sum_{j=1}^{h_a}\sum_{k=1}^{4} e(i,j,k)$$

References

[1] OMICS International. 2016. The role and impact of fossil fuels in our world. OMICS International. Available at: https://www.omicsonline.org. [Accessed Jan. 2026].

[2] Energy Institute. 2024. World Energy Statistical Review 2024. Energy Institute. Available at: https://www.energyinst.org/statistical-review. [Accessed Jan. 2026].

[3] Statista. 2023. Fossil fuel share in energy consumption 1965–2023. Statista. Available at: https://www.statista.com/statistics/222300/fossil-fuel-consumption-share-worldwide/. [Accessed Jan. 2026].

[4] Wolf, S., Bullard, R., Buonocore, J. J., Donley, N., Farrelly, T., Fleming, J., González, D. J. X., Oreskes, N., Ripple, W., Saha, R., and Willis, M. D. 2025. Scientists' warning on fossil fuels. Oxford Open Climate Change, 5(1), kgaf011.

[5] ClientEarth. 2024. Fossil fuels and climate change: The facts. ClientEarth. Available at: https://www.clientearth.org/latest/news/fossil-fuels-and-climate-change-the-facts/. [Accessed Jan. 2026].

[6] Nijsse, F. J. M. M., Mercure, J. F., Sharpe, S., and Ives, M. C. 2023. The momentum of the solar energy transition. Nature Communications, 14(1), 1–15.

[7] Maka, A. O. M. and Alabid, J. M. 2022. Solar energy technology and its roles in sustainable development. Clean Energy, 6(3), 476–483.

[8] Li, X., Wang, Y., and Zhang, Z. 2025. Renewable energy capacity and technological innovations. Environmental Progress, 44(2), 100–112.

[9] Wang, K.-J., Makond, B., and Liu, S.-Y. 2011. Location and allocation decisions in a two-echelon supply chain with stochastic demand—A genetic-algorithm-based solution. Expert Systems with Applications, 38(5), 6125–6131.

[10] Wang, K.-J. and Dao, L. D. 2020. Multiple-objective optimization for solar concentrator layout. Journal of Solar Energy Engineering, 142(1), 011009.

[11] Wang, K.-J., Dung, N. D. T., and Whang, A. J.-W. 2014. Prism-based sunlight concentrator layout: A genetic algorithm solution. Journal of Solar Energy Engineering, 136(2), 021016.

[12] Wang, K. J. and Yang, J. W. 2014. Sunlight concentrator design using a revised genetic algorithm. Renewable Energy, 72, 322–335.

[13] Wikipedia contributors. 2026. Snell's law. Wikipedia, The Free Encyclopedia. Available at: https://en.wikipedia.org/wiki/Snell%27s_law. [Accessed Jan. 2026].

[14] Kim, G. and Moon, I. 2021. Integrated planning for product selection, shelf-space allocation, and replenishment decision with elasticity and positioning effects. Journal of Retailing and Consumer Services, 58, 102274.

[15] Regateiro, F., Bento, J., and Dias, J. 2012. Floor plan design using block algebra and constraint satisfaction. Advanced Engineering Informatics, 26(2), 361–382.

[16] Oduguwa, V. and Roy, R. 2002. Bi-level optimisation using genetic algorithm. In Proceedings of the 2002 IEEE International Conference on Artificial Intelligence Systems (ICAIS), pp. 322–327.

[17] Gusain, C. et al. 2023. Study of meta-heuristic optimization methodologies for solving optimization problems. SoftwareX, 22, 101346.

[18] Benaissa, B. and Kobayashi, M. 2024. Metaheuristic optimization algorithms: An overview. Journal of Sciences - ACS, 14(1), 166–179.

[19] Santoso, T., Ahmed, S., and Shapiro, A. 2019. A Python package for multi-stage stochastic programming. Optimization-Online, Technical Report. Available at: http://www.optimization-online.org. [Accessed Jan. 2026].

[20] Santoso, T., Ahmed, S., Goetschalckx, M., and Shapiro, A. 2005. A stochastic programming approach for supply chain network design under uncertainty. European Journal of Operational Research, 167(1), 96–115.

[21] Numba Development Team. 2025. Numba: A high-performance Python compiler. Available at: https://numba.readthedocs.io/en/stable/. [Accessed Jan. 2026].

[22] De Rainville, F.-M., Fortin, F.-A., Parizeau, M., and Gagné, C. 2012. DEAP: A Python framework for evolutionary algorithms. In Proceedings of the 14th Annual Conference Companion on Genetic and Evolutionary Computation (GECCO), New York, NY, USA, pp. 85–92.

[23] DEAP Development Team. 2025. DEAP: Distributed evolutionary algorithms in Python, version 1.4.3. Available at: https://deap.readthedocs.io/en/master/. [Accessed Jan. 2026].

[24] Fortin, F.-A., De Rainville, F.-M., Gardner, M.-A., Parizeau, M., and Gagné, C. 2012. DEAP: Evolutionary algorithms made easy. Journal of Machine Learning Research, 13, 2171–2175.

[25] Holland, J. H. 1975. Adaptation in Natural and Artificial Systems: An Introductory Analysis with Applications to Biology, Control, and Artificial Intelligence. Ann Arbor, MI: University of Michigan Press.

[26] Zomaya, A. Y. and Kazman, R. 2010. Simulated annealing techniques. In Tucker, A. B. (Ed.), Computer Science and Engineering Handbook, 2nd ed. Boca Raton, FL: CRC Press, pp. 33-1–33-16.

[27] Kirkpatrick, S., Gelatt, C. D., and Vecchi, M. P. 1983. Optimization by simulated annealing. Science, 220(4598), 671–680.

[28] Kennedy, J. and Eberhart, R. 1995. Particle swarm optimization. In Proceedings of the IEEE International Conference on Neural Networks (ICNN'95), vol. 4, Perth, WA, Australia, pp. 1942–1948.

[29] Leung, Y., Gao, Y., and Xu, Z. 1997. Degree of population diversity—A perspective on premature convergence in genetic algorithms and its Markov chain analysis. IEEE Transactions on Neural Networks, 8(5), 1165–1176.

[30] Hassanat, A. B., Prasath, V. B. S., Al-Msaid, H., and Abu-Qdari, S. A. 2013. Reducing premature convergence problem in genetic algorithm: Application on travel salesman problem. Computer and Information Science, 6(1), 47–55.